Ab Initio Quantum Mechanical Charge Field Molecular Dynamics Simulation (QMCF-MD) of Bi3+ in Water

ARTICLE *in* THE JOURNAL OF PHYSICAL CHEMISTRY A · JULY 2012

Impact Factor: 2.69 · DOI: 10.1021/jp301569k · Source: PubMed

6 AUTHORS, INCLUDING:

Ajmal Khan
COMSATS Information Technology Center – CITC
103 PUBLICATIONS **487** CITATIONS

SEE PROFILE

Reaz Uddin
University of Karachi
25 PUBLICATIONS **299** CITATIONS

SEE PROFILE

THE JOURNAL OF PHYSICAL CHEMISTRY A

Article

pubs.acs.org/JPCA

Ab Initio Quantum Mechanical Charge Field Molecular Dynamics Simulation (QMCF-MD) of Bi^{3+} in Water

Ajmal Khan,[†,‡] Alexander K. H. Weiss,[†] Reaz Uddin,[†,§] Bernhard R. Randolf,[†] Bernd Michael Rode,[†] and Thomas S. Hofer*[,†]

[†]Institute of General, Inorganic, and Theoretical Chemistry, University of Innsbruck, Innrain 52a, A-6020 Innsbruck, Austria

[‡]H. E. J. Research Institute of Chemistry, International Center for Chemical and Biological Sciences, University of Karachi, Karachi-75270, Pakistan

[§]Dr. Panjwani Center for Molecular Medicine and Drug Research, International Center for Chemical and Biological Sciences, University of Karachi, Karachi-75270, Pakistan

ABSTRACT: The hydration of the Bi(III) ion was determined via an ab initio quantum mechanical charge field molecular dynamics (QMCF-MD) simulation. Ten picosecond sampling was carried out to determine structural and dynamical properties of the Bi(III) ion in aqueous solution. In the first hydration shell, the ion is 9-fold coordinated with a maximum probability of the Bi−O distance at 2.51 Å. In total, 11 exchanges were observed in the first-shell showing associative, dissociative, and interexchange character. As with the dominant existence of 9-fold coordination, the geometry of the Bi(III) ion is in between the tricapped trigonal prism and the capped square antiprism.

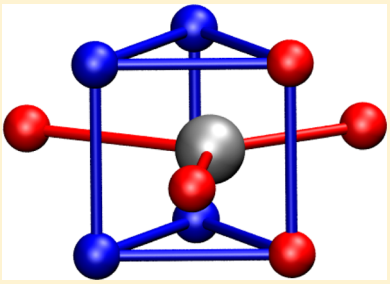

1. INTRODUCTION

Bismuth compounds are used extensively in medical applications, ranging from gastrointestinal disorders to the treatment of kidney stones.[1−6] Bismuth is also used in radiotherapy for cancer, and recent efforts have identified bioactive bismuth complexes with applications in oncology and the treatment of HIV.[7−10] This broad utility makes the study of the behavior of bismuth ions in an aqueous environment imperative.

Concurrent developments in computer speed and capacity have paved the way for simulation techniques using combined ab initio quantum mechanical and molecular mechanical (QM/MM) simulations, and the recently developed quantum mechanical charge field molecular dynamics (QMCF MD) approach[11,12] has been found to be suitable for the study of composite and asymmetrically hydrated ions, mainly because of the inclusion of both primary and secondary hydration layers in the QM treatment.

Structural information on hydrated Bi^{3+} in aqueous solutions has been reported from experimental studies, producing highly variable coordination numbers (3−10), often associated with an irregular coordination geometry.[2] This, together with a visible lone pair effect in certain complexes appears to be a characteristic of Bi(III) as its strong acidity corresponding to a pK_a value of 1.51 in aqueous solution.[13] The rate of ligand exchange at Bi(III) was reported highly variable and dependent upon the pH of the solution.[2] Generally, the structures of Bi(III) compounds are similar to those of As(III) and Sb(III) compounds. The structures of the aquocomplexes of the lanthanide ions $[Ln(H_2O)_9](SO_3CF_3)_3$ and of $[Bi(H_2O)_9]^{3+}$[2,14] are similar. On the basis of their experimental studies, Frank et al.[14] concluded that bismuth coordinates to nine water molecules forming a tricapped trigonal prismatic structure without recognizable stereochemical activity of the lone pair of electrons. Persson et al.[15] proposed that bismuth(III) has coordination number eight in acidic aqueous solution. Previously, we addressed this topic by classical molecular dynamics simulation of Bi^{3+}, which was in favor of the conclusion that bismuth coordinates to nine water molecules forming a tricapped trigonal prismatic structure.[16] In the present work, the hydration of Bi(III) is further investigated employing the quantum mechanical charge field (QMCF) approach. The main aims of this work are elucidating the hydration behavior of Bi^{3+} paying close attention to solvent reorganizational patterns and dynamics.

2. METHODS

The quantum mechanical charge field (QMCF) molecular dynamcs (MD) approach[11,12,17] is, similar as conventional quantum mechanics/molecular mechanics (QM/MM) methods,[18,19] based on the partition of the simulation system. The chemically most relevant part is described by a quantum mechanical technique, and the remaining part is treated by means of classical mechanics. The main difference between these two simulation techniques is the QM region, which, in the case of the QMCF approach, is larger and consists of 2 subregions: the core zone and the solvation layer. The core region contains the solute and the first hydration shell, and the

Received: February 16, 2012
Revised: June 28, 2012
Published: July 2, 2012

dx.doi.org/10.1021/jp301569k | J. Phys. Chem. A 2012, 116, 8008−8014

solvation layer includes another shell of solvent molecules. In conventional QM/MM simulations, the construction of suitable solute−solvent potentials is a time-consuming and sometimes infeasible step. Because of the large radius of the QM region, non-Coulombic interactions between the molecules located in the core region and in the MM zone are negligible, and thus, this method does not require the construction of any other potential functions except those for solvent−solvent interactions. The forces within the different subregion are given as follows:

$$F_J^{\text{core}} = F_J^{\text{QM}} \tag{1}$$

$$F_J^{\text{layer}} = F_J^{\text{QM}} + \sum_{I=1}^{M} F_{IJ}^{\text{BJH}-n\text{C}} \tag{2}$$

$$F_J^{\text{MM}} = \sum_{\substack{I=1 \\ I\neq J}}^{M} F_J^{\text{BJH}} + \sum_{I=1}^{N_1+N_2} \frac{q_I^{\text{QM}} q_J^{\text{QM}}}{r_{IJ}^{\,2}} + \sum_{I=1}^{N_2} F_{IJ}^{\text{BJ}} \tag{3}$$

The forces acting on a particle J in the core zone F_J^{core} are treated quantum mechanically (eq 1). In the solvation layer, the quantum mechanical forces are supplemented by the interactions of the particles with the MM atoms obtained from the BJH−CF2 water model[20,21] (eq 2). In the MM region, the forces are composed of the forces of the BJH−CF2 water model augmented by the Coulombic forces exerted by all atoms in the core region (N_1) and the solvation layer (N_2), and the non-Coulombic forces exerted by all atoms in the solvation layer (N_2) (eq 3). For the calculation of the QM/MM Coulomb contributions, the partial charges of the particles in the QM region are obtained via Mullikan population analysis,[22] which has proven most compatible with the BJH−CF2 water model.[23] The influence of the particles in the MM region onto the QM region is taken into account via a perturbation term of the core Hamiltonian:

$$\hat{H}_{\text{CF}} = \hat{H}_{\text{HF}} + \hat{V} \tag{4}$$

with

$$\hat{V} = \sum_{J=1}^{M} \frac{q_J}{r_{I,J}} \tag{5}$$

where M is the number of particles in the MM zone and q_J the partial charges of these atoms. To guarantee a smooth transition of the molecules between the solvation layer and the MM region, a smoothing function is employed for the atoms of the molecules located in the so-called smoothing region (usually 0.2 Å thick):

$$F_J^{\text{smooth}} = S(r)(F_J^{\text{layer}} - F_J^{\text{MM}}) + F_J^{\text{MM}} \tag{6}$$

where

$$S(r) = \begin{cases} 1 & \text{for } r \le r_1 \\ \dfrac{(r_0^{\,2} - r^2)^2(r_0^{\,2} - 2r^2 - 3r_1^{\,2})}{(r_0^{\,2} - r_1^{\,2})^3} & \text{for } r_1 < r \le r_0 \\ 0 & \text{for } r > r_0 \end{cases} \tag{7}$$

r is the distance of a given solvent molecule (center of mass) from the center of the QM region, r_0 the radius of the QM region, and r_1 the inner border of the smoothing region.

The choice of the basis set is a crucial step for QMCF MD simulations. While the DZP basis set (Dunning)[24] was used for oxygen and hydrogen, different basis sets (LANL2DZ ECP,[25] SBKJC ECP,[26] Def2-SV(P),[27] and cc-pVDZ-PP[28]) were tested for bismuth(III) by performing geometry optimizations for $[Bi(H_2O)_n]^{3+}$ (n = 1−9) species in the gas phase with the software package Gaussian09.[29]

All basis sets delivered good results concerning binding energies and Bi−O distances. The cc-pVDZ-PP[28] basis set was chosen for this simulation based on its favorable computation time. To estimate the effect of electron correlation during the simulation, cluster calculations at HF, MP2, B3LYP, and CCSD levels were performed (Tables 1). The average ion−oxygen bond distances calculated by HF show a negligible difference compared to the MP2 and CCSD method. In the case of the semiempirical B3LYP[30] approach, the effect of electron correlation was overestimated and the difference became more significant. As HF is computationally affordable at present, it was to be preferred and therefore used for this simulation.

Table 1. Bond Distances in Å Obtained from Cluster Calculations at HF, MP2, CCSD, and B3LYP Levels

number of water molecules	HF	MP2	CCSD	B3LYP
1	2.18	2.18	2.18	2.19
2	2.31	2.27	2.30	2.31
3	2.26	2.26	2.26	2.27
4	2.26	2.26	2.26	2.28
5	2.40	2.39		2.40
6	2.18	2.43		2.43
7	2.46	2.43		2.45
8	2.53	2.50		2.51
9	2.61	2.57		2.59

3. SIMULATION PROTOCOL

For the QMCF MD simulation, a cubic box with side length of 31.1 Å was used, containing one Bi^{3+} ion and 1000 water molecules. Periodic boundary conditions were employed and a canonical (NVT) ensemble was chosen, whose temperature was kept constant at 298.15 K using the Berendsen algorithm[31] (relaxation time 0.1 ps). The density of the system was fixed at 0.997 g cm^{-3}, which is the density of pure water at 298.15 K. For the description of the MM water molecules, the flexible BJH−CF2 water model[21] was used, which has proven in previous simulations that a continuous transition between QM and MM regions are granted. To solve the equations of motion, a predictor−corrector algorithm with a 0.2 fs time step was employed. The radius of the core zone was set to 3.0 Å, and the solvation layer ranged from 3.0 to 5.7 Å. The smoothing function extended from 5.5 to 5.7 Å. To correct the cutoff of long-range electrostatic interactions, the reaction field method was employed.[32] Sampling was performed every fifth step, and the whole simulation time was 10 ps. As a starting geometry, the final geometry of a previous MM simulation of Bi(III) in aqueous solution was taken.

The system was characterized by radial distribution functions (RDF), angular distribution function (ADF), and coordination distribution functions (CND). In addition, as all particle coordinates are available at each frame in the simulation trajectory, the local density corrected three-body distribution function[33] was employed to investigate solvent reorganizational

dx.doi.org/10.1021/jp301569k | J. Phys. Chem. A 2012, 116, 8008−8014

patterns around the Bi^{3+} ion. The type of higher order correlation available by this analysis is particularly suited for studying triangular codisposition of particles from which certain organizational motifs can be deduced. Figure 1 illustrates the

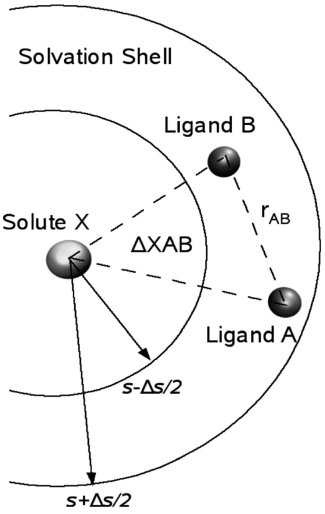

Figure 1. Basic scheme of the analysis of the three-particle distribution, $f^{(3)}_{O-X-O}(s,r,s)$.

basic scheme of the analysis. Briefly, the three-particle distribution, $f^{(3)}_{O-X-O}(s,r,s)$ can be computed as

$$f^{(3)}_{O-X-O}(s, r, s) = \frac{n(s, r, r)}{8\pi^2 N_X \rho_{shell}{}^2 r s^2 \Delta s^2 \Delta r} \quad (8)$$

where N_X is the number of species X and $n(s,r,s)$ is the average number of O−X−O triples with X−O distances ranging from $s - (\Delta s/2)$ (inner border of the shell) to $s + (\Delta s/2)$ (outer border of the shell). ρ_{shell} is the average density of the shell:

$$\rho_{shell} = \sqrt{\frac{N_{shell}(N_{shell} - 1)}{V_{shell}{}^2}} \quad (9)$$

The local density corrected three-body distribution functions were evaluated in order to obtain qualitative and quantitative information about the solvent structure in a given solvation shell by comparing it to the bulk structure.

Besides structural properties such as radial distribution functions, coordination numbers, and various angle distributions, dynamical properties, in particular, mean residence times of ligand molecules, as well as the ion−oxygen stretching frequency were evaluated

The mean residence time (MRT) of ligands in a certain shell was calculated by the direct method:[34]

$$\tau^{0.5} = \frac{t_{sim} N_{av}}{N^{0.5}_{ex}} \quad (10)$$

where t_{sim} is the duration of the simulation, N_{av} is the average number of particles in the respective shell and $N^{0.5}_{ex}$ is the number of registered exchanges with a ligand displacement time of more than 0.5 ps, which corresponds to the mean lifetime of a hydrogen bond, determined by femtosecond laser-pulse spectroscopy.[35] R_{ex}, which indicates the number of exchange attempts needed for a successful exchange, is given by the ratio of the total number of exchange attempts (minimum displacement time 0.0) and the number of exchanges with a displacement of more than 0.5 ps (eq 11).

$$R_{ex} = \frac{N^{0.0}_{ex}}{N^{0.5}_{ex}} \quad (11)$$

Velocity autocorrelation functions (VACFs) $C(t)$ give direct insight into the dynamics of a fluid system as the time integrals are related to macroscopic transport coefficients, and their Fourier transformations are related to vibrational spectra

$$C(t) = \frac{\sum_I^{N_t} \sum_J^N \mathbf{v}_J(t_I)\mathbf{v}_J(t_I + t)}{N_t N \sum_I^{N_t} \sum_J^N \mathbf{v}_J(t_I)\mathbf{v}_J(t_I)} \quad (12)$$

The vibrational power spectra were evaluated using velocity autocorrelation functions according to eq 12 where N is the number of particles, N_t is the number of time origins t_I, and $\mathbf{v}_J$ denotes a certain velocity component of particle J. The power spectrum of the VACF was calculated by Fourier transformation. A correlation length of 1.0 ps was used to obtain the power spectra with 1000 averaged time origins.

In Hartree−Fock calculations, the frequencies are often scaled by a factor of 0.89[36] in order to correct the missing treatment of electron correlation and the influence of the vacuum environment. In this study, the values were not scaled by this factor, as this simulation provided a solvent environment and the influence of electron correlation is small.

4. RESULTS AND DISCUSSION

The radial distribution functions for Bi−O and Bi−H are shown in Figure 2. There are two well-defined hydration shells,

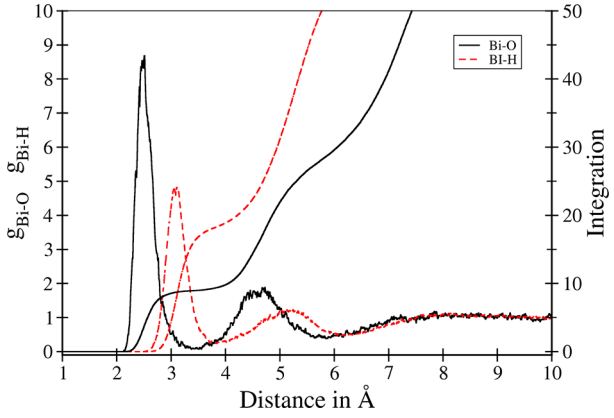

Figure 2. Bi−O (solid line) and Bi−H (dashed line) radial distribution functions and their running integration numbers for Bi(III) in aqueous solution.

and even beyond the second shell, there seems to be a slight ordering of water molecules. A sharp Bi−O peak was observed for the first hydration shell at 2.51 Å, which is in agreement with the Bi−O distance of 2.58 Å evaluated by Frank et al.[14] via X-ray diffraction. Large-angle-X-ray scattering (LAXS) and extended-X-ray-absorption-fine structure (EXAFS) data of a 2−3 mol dm^{-3} $[Bi(H_2O)_9](CF_3SO_3)_3$ solution produced a mean Bi−O bond distance of 2.49 Å for a nine-coordinated ion, but concentration and counterions certainly influence this value.[15] This calculated Bi−O bond distance is also very close to the experimentally calculated value 2.48 Å reported by Sundvall from neutron diffraction for the complex $[Bi_6O_4(HO)_4]^{6+}$.[37] A

dx.doi.org/10.1021/jp301569k | J. Phys. Chem. A 2012, 116, 8008−8014

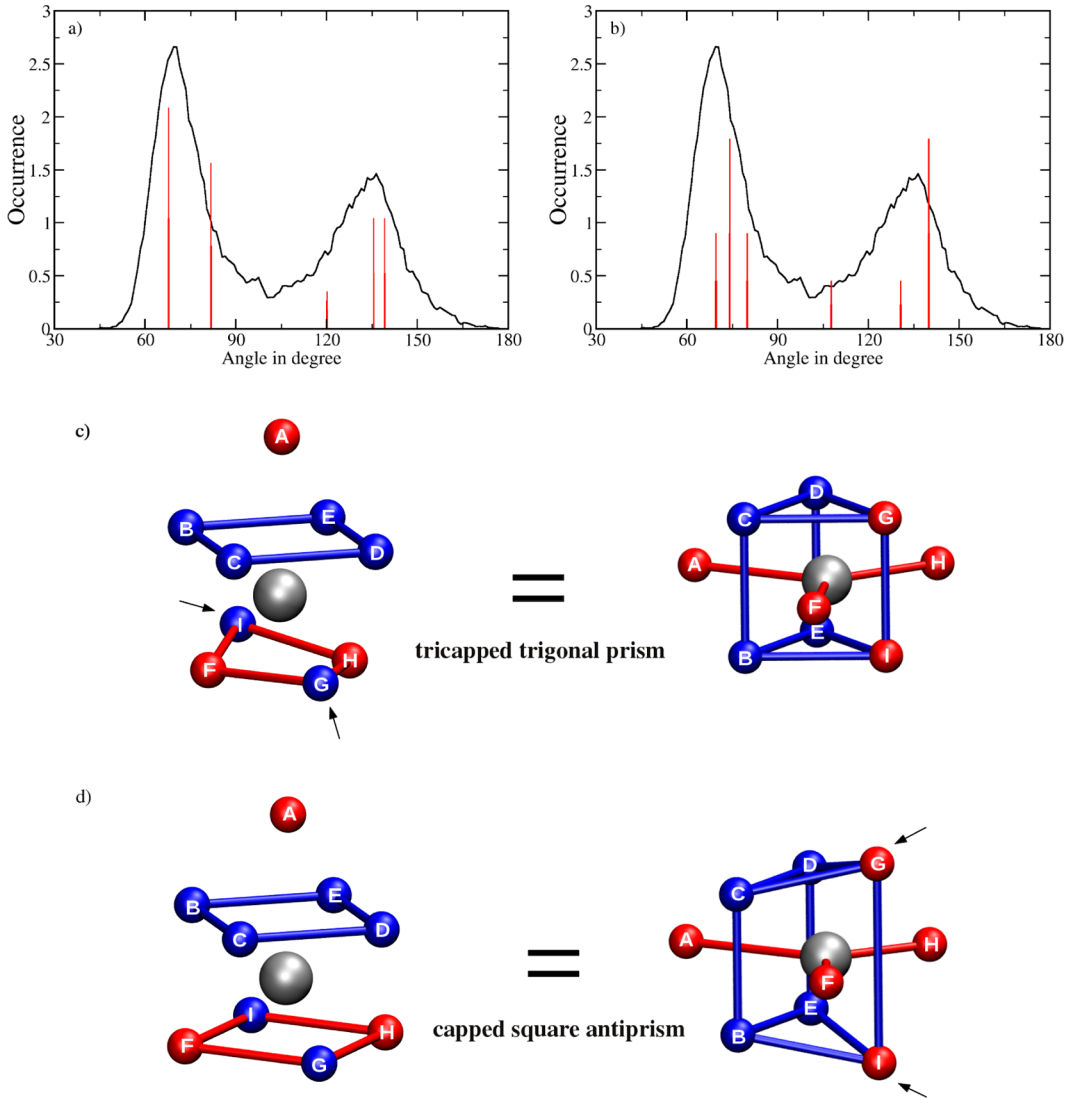

Figure 3. Angular distribution function of the O−Bi−O angle in the first hydration shell superimposed with the expected pattern of (a) a tricapped trigonal prism (ttp) and (b) a capped square antiprism (csp). The similarities of these two structures are demonstrated for (c) the ttp- and (d) csp-geometries, respectively. The left side of panels c and d highlight the csp-structure via the bonds, while the coloring reflects a ttp-alignment. Similarly, the right-hand side of panels c and d depict the ttp-arrangement via bonds, while the coloring of the ligands reflects the csp-structure.

peak at 3.10 Å for the first hydration shell was found in the Bi−H RDF. Although the first shell peaks of Bi−O and Bi−H overlap at 2.81 Å, a strong dipole orientation is present in the first shell. For the second shell, a peak maximum was found at a distance of 4.60 Å and 5.2 Å for the Bi−O and Bi−H RDFs, respectively. The nonzero minimum between the first and second shell in the Bi−O RDF at 3.5 Å indicates that ligand exchanges occurred along the simulation.

Angular distribution functions (ADF) are helpful tools to obtain additional information about hydration structures. Figure 3a,b shows the distribution of the O−Bi−O angle within the first hydration shell superimposed with the angular pattern expected for a tricapped trigonal prism (ttp) and a capped square antiprism (csp), respectively. The ADF peaks at 69.9° and 136.4°, and a minimum is observed at 101°. As this system is extremely dynamic, a prediction of an exact geometric stereotype within the first-shell is difficult. A comparison of the ideal ttp- and csp-structures demonstrating the subtle difference between these structural stereotypes is included in Figure 3c,d. On the left side of Figure 3c,d, both of the systems are depicted from the viewpoint of a csp-arrangement (the bonds highlight the two planes in the csp-structure, while the coloring of atoms reflect the ttp-alignment). For an ideal tricapped trigonal prism (Figure 3c), the main structural difference is visible for the plane formed by atoms F to I; in this case, atoms F and H are tilted away from the plane (Figure 3c left). Similarly, the right side of Figure 3c,d depicts the same structures from the viewpoint of a ttp-arrangement (the bonds highlight the ttp-structure, while the coloring of atoms reflect the csp-arrangement). Here, the main difference is visible in the csp case; the elongation of the distance of atoms G and I, along with a minor rearrangement of the angle between atoms F and H, is sufficient to transform the ttp-structure to a csp-arrangement. The root-mean-square deviation between ideal csp- and ttp-structures with a mean bond distance of 2.49 Å is 0.369 Å, which is small compared to the broadening of the first shell peak of the Bi−O RDF having widths of 0.356 and approximately 0.9 Å at half-maximum and the *x*-axis, respectively. Considering these subtle differences between the structures and the high mobility of the solvent molecules, it can

dx.doi.org/10.1021/jp301569k | *J. Phys. Chem. A* 2012, 116, 8008−8014

be concluded that the system rarely assumes configurations corresponding to these idealized geometries but forms distorted, flexible hydration complexes. An unambiguous assignment to any of the two lead geometries is thus very difficult, and considering the structural similarities between the ttp- and csp-geometries, such a differentiation appears not to be meaningful for the liquid state.

The coordination number distributions of hydrated Bi^{3+} obtained from our simulation are displayed in Figure 4. The

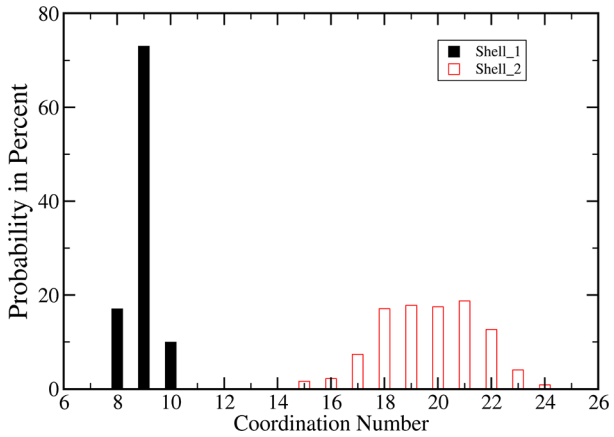

Figure 4. Coordination number distributions of the first and second hydration shell of Bi(III) in aqueous solution obtained from a QMCF MD simulation.

CND (Figure 4) analysis of our current QMCF MD simulation showed that 9-fold coordination is dominant in the whole simulation trajectory. As discussed earlier the geometry in the first-shell is in between capped square antiprism and tricapped trigonal prism. Eight-fold (17%) and 10-fold (10%) coordination complexes were formed in our simulation. In our previous MM/MD simulations of Bi^{3+}, 100% occurrence of coordination number nine was observed,[16] forming a tricapped trigonal prism.[16] For the second hydration shell, a broad coordination number distribution ranging from 15 to 24 with an average of 20 was found.

For a more detailed analysis of the structure, the local density corrected three-body distribution functions ($f^{(3)}_{O-X-O}(s,r,s)$) were calculated (Figure 5) for different hydration shells obtained from the ion−oxygen RDF. For the first hydration

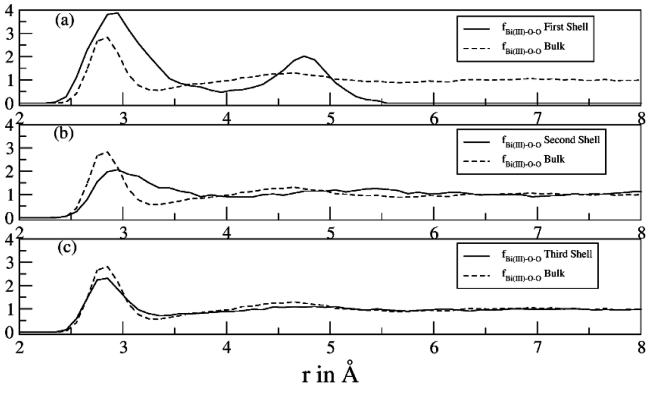

Figure 5. Local density corrected three-body distributions for the first (a), second (b), and third (c) shells of Bi(III) (solid line), compared with that of bulk (dashed line).

shell, the function shows two sharp peaks at positions 2.9 Å and 4.7 Å (Figure 5a). The arrangement of water molecules in this shell differs significantly from the arrangement in the bulk. The influence of the ion on the second shell's water molecules is also pronounced (Figure 5b), as almost no oxygen−oxygen distances of 2.88 Å (peak maximum of the reference function for the bulk) were found. This indicates that very few hydrogen bonds exist between the water molecules inside this shell. For the third shell's function (Figure 5c), a peak at 2.8 Å was found, but as this peak is not as high as in the reference function, there is still some ordering effect of the Bi(III) ion at this distance, the water dipoles slightly orientate with the negative partial charge toward the ion. It can be concluded that the Bi(III) ion has no influence on the water structure beyond the third shell.

The indications toward ligand exchange processes from the radial distribution functions as well as the different coordination numbers obtained from the CND called for a more detailed investigation of the exchange dynamics. Since detailed information on water exchange between hydration shells of ions and bulk is fundamental to describe the reactivity of ions, it was of special interest to evaluate the mean lifetime of the first shell ligands connected to these exchange processes. In this work, the mean residence time (MRT) values were calculated using a direct evaluation of exchange events,[34] accepting only ligand displacements lasting longer than 0.5 ps as a successful exchange event. The ion−oxygen distances of all first shell molecules showing lasting exchanges (≥0.5 ps) obtained from the QMCF MD simulation are depicted in Figure 6. Taking into account the varying coordination numbers and MRT data, it can be concluded that Bi(III) induces fast ligand movements.

During the simulation time of 10 ps, a number of ligand exchange reaction was observed (see Figure 6), where the ligands cross the borderline between the first and second shells at 3.38 Å. For up to 1.35 ps, Bi(III) is 9-fold coordinated. The first exchange event was observed at 1.35 ps by the entering of a ligand into the first shell leading to a 10-fold coordination. This hydration pattern was maintained for a very short time until another ligand left the first-shell at 1.88 ps, re-establishing a 9-fold coordination. This exchange followed an associative exchange mechanism. Shortly thereafter, at 2.25 ps, another ligand exchange occurs following an interchange mechanism, i.e., both ligands enter and leave the hydration shell simultaneously. The third type of mechanism referred to as dissociative exchange mechanism was observed between 3.5 and 4.5 ps, where, in the first step, a ligand left the hydration shell leading to an 8-fold coordination. Next, another solvent molecule entered, re-establishing a 9-fold hydration pattern. Another dissociative exchange process (7−8.5 ps) and two more interchange events (7.8 and 9.6 ps) were observed within the simulation. These findings clearly demonstrate that ligand exchange is not restricted to an exclusive mechanism and that all three stereotypes of the exchange mechanism (associative, dissociative, and interchanges)[38] can occur within the same system in short time.

Table 2 lists some of the most important dynamical parameters such as the number of ligand exchange processes, the mean ligand residence times, and the sustainability of migration processes.

The strong ion−ligand bonding deduced from the structural properties is reflected in the Bi(III)−O vibrational mode as well. The frequency of the Bi(III)−O stretching motion peaks at 312 cm^{-1}; the corresponding force constant is 85.1 N/m. This frequency is very close to experimental values given as 311

dx.doi.org/10.1021/jp301569k | J. Phys. Chem. A 2012, 116, 8008−8014

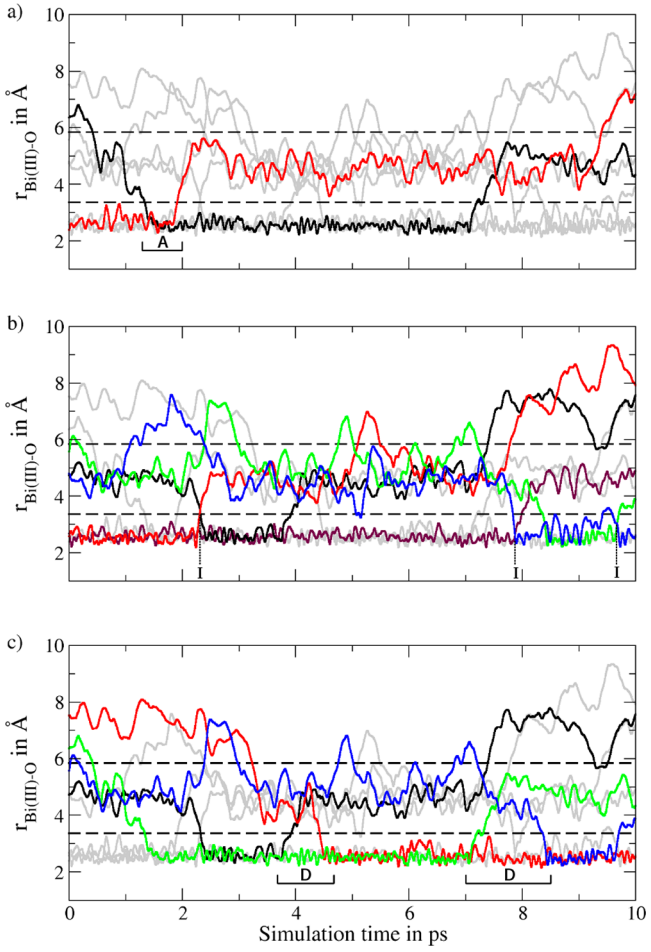

Figure 6. Ion−O distances of all first shell ligands showing persisting exchanges (≥0.5 ps) obtained from the QMCF MD simulations. The highlighted plots correspond to (a) associative (A), (b) interchange (I), and (c) dissociative (D) exchanges events, respectively.

Table 2. Ligand Exchange Parameters Obtained from the QMCF-MD Simulation of Bi^{3+} in Aqueous Solution[a]

	CND_{av}	$\tau^{0.5}$	$N_{ex}^{0.5}$/10 ps	$N_{ex}^{0.0}$/10 ps	R_{ex}
1st shell	8.93	8.13	11	26	2.36
2nd shell	19.68	1.76	112	293	2.62

[a]Here, CND_{av} are average numbers of coordination for 1st and 2nd shells. τ is the mean ligand residence time in ps. $N_{ex}^{0.5}$and $N_{ex}^{0.0}$ are the number of accounted exchange events per 10 ps lasting at least 0 and 0.5 ps, respectively. R_{ex} is average number of processes needed for one successful ligand exchange.

cm^{-1} reported by Hardcasle et al.[39] and 314 cm^{-1} by Narang et al.[40] from X-ray diffraction for bismuth oxides, while 313 cm^{-1} reported by Salazar-Perez et al.[41] from HR-TEM, X-ray diffraction, and microraman spectroscopy of bismuth oxides. The frequency obtained from our QMCF-MD simulation is also in close agreement with the calculated Bi−O frequencies reported by Pye et al. from an ab initio investigation of bismuth hydration as 303−315 cm^{-1} for 9-fold coordination of Bi(III).[42]

Other trivalent ions investigated within the same methodical framework show much higher vibration frequencies, resulting in force constants of 144, 211, 174, 144, and 174 N/m for Al(III),[43] Ti(III),[44] Cr(III),[45] Fe(III),[46] and Co(III),[47] respectively. Previously, we had calculated the frequencies for La(III)[48] and Ce(III)[49] with force constants of 54.3 N/m and 73 N/m, respectively, which are also lower than the above-mentioned trivalent ions.

5. CONCLUSIONS

The hydration behavior and dynamics of Bi(III) were calculated by ab initio (QMCF-MD) simulation. In this article a QMCF-MD simulation of Bi(III) was carried out up to 10 ps, which showed a predominating 9-fold coordination. The distance of Bi−O and the frequency were found in excellent agreement to experimental data. Despite its trivalent charge, this system is very dynamic and a total of 11 exchanges in the first shell and 112 exchanges in the second shell occurred with associative exchange, dissociative exchange, and interchange characteristics. This work demonstrated that different stereotypes of exchanges can be observed within the same system in very short time.

AUTHOR INFORMATION

Notes

The authors declare no competing financial interest.

REFERENCES

(1) Committee for Veterinary Medicinal Products−Summary Reports (1), The European Agency for the Evaluation of Medicinal Products, Veterinary Medicines Evaluation Unit, 1997.
(2) Sadler, P. J.; Li, H.; Sun, H. *Coord. Chem. Rev.* **1999**, *185−186*, 689−709.
(3) Lambert, J. R.; Midolo, P. *Aliment. Pharmacol. Ther. Suppl.* **1997**, *11*, 27−33.
(4) Briand, G. G.; Burford, N. *Chem. Rev.* **1999**, *99*, 2601−2658.
(5) Sun, H.; Zhang, L.; Szeto, K. Y. *Metal. Ions Biol. Syst.* **2004**, *41*, 333−378.
(6) Zhang, L.; Mulrooney, S. B.; Leung, A. F. K.; Zeng, Y.; Ko, B. B. C.; Hausinger, R. P.; Sun, H. *BioMetals* **2006**, *19*, 503−511.
(7) Kozak, R. W.; Waldmann, T. A.; Atcher, R. W.; Gansow, O. A. *Trends. Biotechnol.* **1986**, *4*, 259−264.
(8) Kozak, R. W.; Atcher, R. W.; Gansow, O. A.; Friedman, A. M.; Hines, J. J.; Waldmann, T. A. *Proc. Natl. Acad. Sci. U.S.A.* **1986**, *83*, 474−478.
(9) Kirschner, S.; Wei, Y. K.; Francis, D.; Bergman, J. G. *J. Med. Chem.* **1966**, *9*, 369−372.
(10) Mahmood, N.; Burke, A.; Hussain, S.; Anner, R. M.; Anner, B. M. *Antiviral Chem. Chemother.* **1995**, *6*, 187−189.
(11) Rode, B. M.; Hofer, T. S.; Randolf, B. R.; Schwenk, C. F.; Xenides, D.; Vchirawongkwin, V. *Theor. Chim. Acta.* **2006**, *115*, 77−85.
(12) Hofer, T. S.; Pribil, A. B.; Randolf, B. R.; Rode, B. M. *Adv. Quantum Chem.* **2010**, *59*, 213−246.
(13) Pettit, G.; Pettit, L. D. *IUPAC Stability Constant Database*; IUPAC and Academic Software: Otley, UK, 1993.
(14) Frank, W.; Reiss, G. J.; Schneider, J. *Angew. Chem., Int. Ed.* **1995**, *34*, 2416−2417.
(15) Näslund, J.; Persson, I.; Sandström, M. *Inorg. Chem.* **2000**, *39*, 4012−4021.
(16) Durdagi, S.; Hofer, T. S.; Randolf, B. R.; Rode, B. M. *Chem. Phys. Lett.* **2005**, *406*, 20−23.
(17) Hofer, T. S.; Rode, B. M.; Pribil, A. B.; Randolf, B. R. *Adv. Inorg. Chem.* **2010**, *62*, 143−175.
(18) Field, M. J.; Bash, P. A.; Karplus, M. *J. Comput. Chem.* **1990**, *11*, 700−733.
(19) Bakowies, D.; Thiel, W. *J. Phys. Chem.* **1996**, *100*, 10580−10594.
(20) Stillinger, F. H.; Rahman, A. *J. Chem. Phys.* **1978**, *68*, 666−670.
(21) Bopp, P.; Jancsö, G.; Heinzinger, K. *Chem. Phys. Lett.* **1983**, *98*, 129−133.
(22) Mulliken, R. S. *J. Chem. Phys.* **1962**, *36*, 3428−3439.
(23) Hofer, T. S.; Randolf, B. R.; Rode, B. M. *J. Phys. Chem.* **2008**, *112*, 11726−11733.
(24) Dunning, T. H., Jr. *J. Chem. Phys.* **1970**, *53*, 2823−2833.
(25) Wadt, W. R.; Hay, P. J. *J. Chem. Phys.* **1985**, *82*, 284−268.

(26) Stevens, W. J.; Krauss, M.; Basch, H.; Jasien, P. G. *Can. J. Chem.* **1992**, *70*, 612−630.
(27) Weigend, F.; Ahlrichs, R. *Phys. Chem. Chem. Phys.* **2005**, *7*, 3297−3305.
(28) Peterson, K. A.; Figgen, D.; Goll, E.; Stoll, H.; Dolg, M. *J. Chem. Phys.* **2003**, *119*, 11113−11123.
(29) Frisch, M. J.; Trucks, G. W.; Schlegel, H. B.; Scuseria, G. E.; Robb, M. A.; Cheeseman, J. R.; Scalmani, G.; Barone, V.; Mennucci, B.; Petersson, G. A.; Nakatsuji, H.; Caricato, M.; Li, X.; Hratchian, H. P.; Izmaylov, A. F.; Bloino, J.; Zheng, G.; Sonnenberg, J. L.; Hada, M.; Ehara, M.; Toyota, K.; Fukuda, R.; Hasegawa, J.; Ishida, M.; Nakajima, T.; Honda, Y.; Kitao, O.; Nakai, H.; Vreven, T.; Montgomery, J. A., Jr.; Peralta, J. E.; Ogliaro, F.; Bearpark, M.; Heyd, J. J.; Brothers, E.; Kudin, K. N.; Staroverov, V. N.; Kobayashi, R.; Normand, J.; Raghavachari, K.; Rendell, A.; Burant, J. C.; Iyengar, S. S.; Tomasi, J.; Cossi, M.; Rega, N.; Millam, J. M.; Klene, M.; Knox, J. E.; Cross, J. B.; Bakken, V.; Adamo, C.; Jaramillo, J.; Gomperts, R.; Stratmann, R. E.; Yazyev, O.; Austin, A. J.; Cammi, R.; Pomelli, C.; Ochterski, J. W.; Martin, R. L.; Morokuma, K.; Zakrzewski, V. G.; Voth, G. A.; Salvador, P.; Dannenberg, J. J.; Dapprich, S.; Daniels, A. D.; Farkas, O.; Foresman, J. B.; Ortiz, J. V.; Cioslowski, J.; Fox, D. J. *Gaussian 09*, revision A.02; Gaussian, Inc.: Wallingford, CT, 2009.
(30) Becke, A. D. *J. Chem. Phys.* **1993**, *98*, 5648−5652.
(31) Berendsen, H. J. C.; Postma, J. P. M.; Van Gunsteren, W. F.; DiNola, A.; Haak, J. R. *J. Chem. Phys.* **1984**, *81*, 3684−3690.
(32) Adams, D. J.; Adams, E. M.; Hills, G. J. *Mol. Phys.* **1979**, *38*, 387−400.
(33) Bhattacharjee, A.; Hofer, T. S.; Rode, B. M. *Phys. Chem. Chem. Phys.* **2008**, *10*, 6653−6657.
(34) Hofer, T. S.; Tran, H. T.; Schwenk, C. F.; Rode, B. M. *J. Comput. Chem.* **2004**, *25*, 211−217.
(35) Lock, A. J.; Woutersen, S.; Bakker, H. *Femtochemistry and Femtobiology*; World Scientific: Singapore, 2001.
(36) Scott, A. P.; Radom, L. *J. Phys. Chem.* **1996**, *100*, 16502−16513.
(37) Sundvall, B. *Inorg. Chem.* **1983**, *22*, 1906−1912.
(38) Helm, L.; Merbach, A. E. *Chem. Rev.* **2005**, *105*, 1923−1960.
(39) Hardcastle, F. D.; Wachs, I. E. *J. Solid State Chem.* **1992**, *97*, 319−331.
(40) Narang, S. N.; Patel, N. D.; Kartha, V. B. *J. Mol. Struct.* **1994**, *327*, 221−235.
(41) Salazar-Perez, A. J.; Camacho-Lopez, M. A.; Morales-Luckie, R. A.; Sanchez-Mendieta, V.; Urena-Nunez, F.; Arenas-Alatorre, J. *Superficies y Vacío* **2005**, *18*, 4−8.
(42) Pye, C. C.; Gunasekara, C. M.; Rudolph, W. W. *Can. J. Chem.* **2007**, *85*, 945−950.
(43) Hofer, T. S.; Randolf, B. R.; Rode, B. M. *Phys. Chem. Chem. Phys.* **2005**, *7*, 1382−1387.
(44) Kritayakornupong, C.; Plankensteiner, K.; Rode, B. M. *ChemPhysChem* **2004**, *5*, 1499−1506.
(45) Kritayakornupong, C.; Plankensteiner, K.; Rode, B. M. *J. Comput. Chem.* **2004**, *25*, 1576−1583.
(46) Remsungnen, T.; Rode, B. M. *Chem. Phys. Lett.* **2003**, *367*, 586−592.
(47) Kritayakornupong, C.; Plankensteiner, K.; Rode, B. M. *J. Chem. Phys.* **2003**, *119*, 6068−6072.
(48) Hofer, T. S.; Scharnagl, H.; Randolf, B. R.; Rode, B. M. *Chem. Phys.* **2006**, *327*, 31−42.
(49) Lutz., O. M. D.; Hofer, T. S.; Randolf, B. R.; Rode, B. M. *Chem. Phys. Lett.* **2012**, *540*, 50−53.